Glycosylated RGD-Containing Peptides: Tracer for Tumor Targeting and Angiogenesis Imaging with Improved Biokinetics

Roland Haubner, Hans-Jürgen Wester, Fred Burkhart, Reingard Senekowitsch-Schmidtke, Wolfgang Weber, Simon L. Goodman, Horst Kessler, and Markus Schwaiger

Department of Nuclear Medicine and Institute of Organic Chemistry and Biochemistry, Technische Universität München, Munich; and Department of Preclinical Oncology, Merck KGaA, Darmstadt, Germany

The $\alpha_V\beta_3$ integrin plays an important role in metastasis and tumor-induced angiogenesis. Targeting with radiolabeled ligands of the $\alpha_V\beta_3$ integrin may provide information about the receptor status and enable specific therapeutic planning. Previous studies from our group resulted in tracers that showed $\alpha_V\beta_3$-selective tumor uptake. However, these first-generation compounds predominantly revealed hepatobiliary excretion with high radioactivity found in the liver. In this report, the synthesis and biological evaluation of the first glycosylated RGD-containing peptide (RGD-peptide) for the noninvasive imaging of $\alpha_V\beta_3$ expression are described. **Methods:** Peptides were assembled on a solid support using fluorenylmethoxycarbonyl-coupling protocols. The precursor cyclo(-Arg-Gly-Asp-D-Tyr-Lys(SAA)-) GP1 was synthesized by coupling 3-acetamido-2,6-anhydro-4,5,7-tri-*O*-benzyl-3-deoxy-β-D-glycero-D-gulo-heptonic acid (SAA(Bn_3)) with cyclo(-Arg(Mtr)-Gly-Asp(OtBu)-D-Tyr(tBu)-Lys-) and subsequent removal of the protection groups. Iodine labeling was performed by the Iodo-Gen method (radiochemical yield > 50%). The in vitro binding assays were performed using purified immobilized $\alpha_{IIb}\beta_3$, $\alpha_V\beta_5$, and $\alpha_V\beta_3$ integrins. For in vivo experiments, nude mice bearing xenotransplanted melanomas and mice with osteosarcomas were used. **Results:** The glycosylated peptide 3-iodo-Tyr^4-cyclo(-Arg-Gly-Asp-D-Tyr-Lys(SAA)-) GP2 showed high affinity and selectivity for $\alpha_V\beta_3$ in vitro (50% inhibitory concentration = 40 nmol/L). Pretreatment studies indicate specific binding of [^{125}I]GP2 on $\alpha_V\beta_3$-expressing tumors in vivo. Comparison of the pharmacokinetics of [^{125}I]GP2 and [^{125}I]-3-iodo-Tyr^4-cyclo(-Arg-Gly-Asp-D-Tyr-Val-) [^{125}I]P2 revealed for [^{125}I]GP2 an increased activity concentration in the blood (e.g., 3.59 ± 0.35 percentage injected dose [%ID]/g vs. 1.72 ± 0.44 %ID/g at 10 min postinjection) and a significantly reduced uptake in the liver (e.g., 2.59 ± 0.24 %ID/g vs. 21.96 ± 2.78 %ID/g at 10 min postinjection). Furthermore, a clearly increased activity accumulation in the tumor was found (e.g., 3.05 ± 0.31 %ID/g vs. 0.92 ± 0.16 %ID/g at 240 min postinjection), which remained almost constant between 60 and 240 min postinjection. This resulted in good tumor-to-organ ratios for the glycosylated tracer (e.g., 240-min postinjection osteosarcoma model: tumor-to-blood = 16; tumor-to-muscle = 7; tumor-to-liver = 2.5), which were confirmed by the first gamma-camera images of osteosarcoma-bearing mice at 240 min postinjection. **Conclusion:** This study demonstrates that the introduction of a sugar moiety improves the pharmakokinetic behavior of a hydrophobic peptide-based tracer. Additionally, this $\alpha_V\beta_3$-selective glycosylated radioiodinated second-generation tracer GP2 shows high tumor uptake and good tumor-to-organ ratios that allow noninvasive visualization of $\alpha_V\beta_3$-expressing tumors and monitoring therapy with $\alpha_V\beta_3$ antagonists. Finally, the favorable biokinetics make the glycosylated RGD-peptide a promising lead structure for tracers to quantify the $\alpha_V\beta_3$ expression using PET.

Key Words: glycosylated RGD-peptides; $\alpha_V\beta_3$ antagonists; integrin; angiogenesis; tumor targeting

J Nucl Med 2001; 42:326–336

Cell matrix interactions are fundamental to tumor invasion and formation of metastases (*1*) as well as to tumor-induced angiogenesis (*2*). The integrins, heterodimeric transmembrane glycoproteins that compose a diverse family of 19 α and eight β subunits, play a key role in these interactions (*3*). In addition to adhesive functions, it is increasingly apparent that integrins transduce messages by classical signaling pathways and may influence proliferation and apoptosis of tumor cells as well as activated endothelial cells (*2,4*).

An integrin with a well-characterized involvement in angiogenesis (*5*) and tumor invasiveness (*6*) is $\alpha_V\beta_3$. This integrin is expressed on various malignant human tumors (*6*) as well as on endothelial cells during neovascularization (*2,7*). Inhibition of the $\alpha_V\beta_3$-mediated cell-matrix interaction leads to apoptosis of activated endothelial cells and disrupts blood vessel formation (*8*). By contrast, $\alpha_V\beta_3$ is not strongly expressed on quiescent endothelial cells. Thus, treatment with $\alpha_V\beta_3$ antagonists did not affect preexisting blood vessels (*9*). In tumor models, inhibition of blood vessel formation using $\alpha_V\beta_3$ antagonists not only blocked tumor-associated angiogenesis but in some cases resulted in tumor regression (*8,10*).

Received Apr. 27, 2000; revision accepted Aug. 14, 2000.

For correspondence and reprints contact: Roland Haubner, PhD, Department of Nuclear Medicine, Klinikum rechts der Isar, Technische Universität München, Ismaninger Strasse 22, D-81675 Munich, Germany.

These encouraging experimental studies have already led to initial clinical trials evaluating the use of $\alpha_V\beta_3$ antagonists as antiangiogenic drugs in patients with various malignant tumors (*11*). However, currently available imaging techniques are limited in monitoring treatment with this class of drug. Antitumor activity is generally assessed by determining the percentage of patients in whom a significant reduction of the tumor size is achieved during a relatively short period of therapy ("response rate"). Thus, this method may not be applicable for a form of therapy that is aimed at disease stabilization and prevention of metastases. Therefore, noninvasive methods to visualize and quantify $\alpha_V\beta_3$ expression in vivo appear to be crucial for the future development and clinical application of $\alpha_V\beta_3$ antagonists in cancer patients (*11*). Using these techniques, it would be possible to determine $\alpha_V\beta_3$-dependent angiogenesis and to recognize those patients most amenable to this kind of therapy.

We have recently described radiolabeled cyclic RGD-peptides with high affinity and selectivity for the $\alpha_V\beta_3$ integrin (*12*). These peptides showed receptor-specific accumulation in different tumor and mouse models. However, they also revealed fast hepatobiliary excretion. The resulting high activity concentration in the liver and intestine limits the application of these tracers for tumor imaging.

The aim of this study was to improve the pharmacokinetics of these $\alpha_V\beta_3$-selective, first-generation tracers to allow noninvasive imaging of $\alpha_V\beta_3$ expression with gamma camera imaging techniques. For this purpose, glycosylation of a modified derivative of these peptides by using a sugar amino acid was evaluated to decrease lipophilicity and hepatic uptake.

MATERIALS AND METHODS

All chemicals were used as supplied without further purification. 9-Fluorenylmethoxycarbonyl (Fmoc) amino acids were purchased from Bachem (Heidelberg, Germany) or Novabiochem (San Diego, CA). Synthesis of Fmoc-3-iodo-D-Tyr-OH was described elsewhere (*12*). The tritylchloride polystyrol (TCP) resin was purchased form PepChem (Tübingen, Germany). 1-Hydroxybenzotriazol (HOBt), *O*-(1H-benzo-triazol-1-yl)-*N*,*N*,*N*′,*N*′-tetramethyluronium tetrafluoroborate, and diphenyl phosphorazidate were purchased from Aldrich (Steinheim, Germany) or Alexis (Grünberg, Germany). 1-Hydroxy-7-azabenzotriazole (HOAt) and *O*-(7-azabenzotriazol-1-yl)-1,1,3,3-tetramethyluronium hexafluorophosphate were purchased from PerSeptive Biosystems (Hamburg, Germany). Sodium iodide-125 and sodium iodide-123 were purchased from Amersham (Buckinghamshire, UK). All other organic reagents were purchased from Merck (Darmstadt, Germany), Aldrich or Fluka (St. Louis, MO).

Mass spectra were recorded on the liquid-chromatography mass-spectrometry system LCQ from Finnigan (Bremen, Germany) using the Hewlett-Packard series 1100 high-performance liquid chromatography system. Nuclear magnetic resonance (NMR) spectra were recorded on a Bruker AC 250 or Bruker AMX 500 (Karlsruhe, Germany) at 300 K. For all experiments, the solvent signal was used for calibration.

Analytical reversed-phase high performance liquid chromatography (RP-HPLC) was performed on Sykam equipment (Gilching, Germany) using columns with YMC-Pack ODS-A (5 μm, 250 $\times$ 4 mm) (YMC Co., Ltd., Kyoto, Japan). For radioactivity measurements, the outlet of the ultraviolet detector was connected to a well scintillation NaI(Tl) detector from EG & G (Munich, Germany). For analytical data, several acetonitrile-water gradients with 0.1% trifluoroacetic acid (TFA) were used.

Preparative RP-HPLC was performed with the Sykam HPLC system. Columns were YMC-Pack ODS-A (5 μm, 250 $\times$ 30 mm) for the reference peptides and precursor and YMC-Pack ODS-A (5 μm, 250 $\times$ 4 mm) for radioactively labeled compounds with the same solvent system as described above.

Synthesis of the Sugar Amino Acids

Synthesis of 3-Acetamido-2,6-Anhydro-4,5,7-Tri-O-*Benzyl-3-Deoxy-β-D-Glycero-D-Gulo-Heptonic Acid.* The benyzl-protected sugar amino acid 3-acetamido-2,6-anhydro-4,5,7-tri-*O*-benzyl-3-deoxy-β-D-glycero-D-gulo-heptonic acid (SAA(Bn_3)) was synthesized according to Hoffmann et al. (*13*).

Synthesis of 3-Acetamido-2,6-Anhydro-3-Deoxy-β-D-Glycero-D-Gulo-Heptonic Acid. SAA(Bn_3) (0.2 mmol) was dissolved in 3.5 mL of a mixture of tetrahydrofuran/methanol (MeOH)/water (3:3:1). After addition of 0.57 mmol palladium oxide and 200 μL acetic acid (HOAc), the suspension was stirred for 48 h under a hydrogen atmosphere at ambient temperature. The suspension was filtered, and the solvent was removed in vacuo. The crude product was freeze-dried with *tert.*butanol (tBu). The sugar amino acid was used without further purification. Deprotection was monitored with RP-HPLC and NMR.

Peptide and Glycopeptide Synthesis

Synthesis of Cyclic Pentapeptides. Loading of the TCP-resin, synthesis of the peptides, and subsequent cyclization were performed by protocols described elsewhere (*12*). Side chains were protected with 4-methoxy-2,3,6-trimethylbenzenesulfonyl (Mtr) or 2,2,4,6,7-pentamethyldihydrobenzofuran-5-sulfonyl (Pbf) for arginine, benzyloxycarbonyl (Z), or 1-(4,4-dimethyl-2,6-dioxocyclohex-1-ylidene)ethyl for lysine and tBu for aspartic acid and tyrosine. Because of the sensitivity of the D-3-iodo-tyrosine to reducing conditions using hydrogen or palladium, two different synthesis routes for the reference peptide and the labeling precursor have been introduced. The resulting peptides are cyclo(-Arg-(Mtr)-Gly-Asp(OtBu)-D-Tyr(tBu)-Lys(Z)-) (peptide precursor for labeling) and cyclo(-Arg(Pbf)-Gly-Asp(OtBu)-D-3-iodo-Tyr-Lys-(Dde)-) (peptide precursor for the reference compound).

Selective Removal of Z-Protection Group. Cyclo(-Arg(Mtr)-Gly-Asp(OtBu)-D-Tyr(tBu)-Lys(Z)-) (1.3 mmol) was dissolved in 20 mL dimethyl acetamide, and 400 μL HOAc and 1 g palladium catalyst (5% Pd on charcoal) were added. The reaction mixture was allowed to stir under hydrogen atmosphere for 6 h at ambient temperature. The solvent was reduced in vacuo, the residue was resuspended in MeOH, and the suspension was filtered. The solvent was reduced, and the residue was triturated with ethyl ether, filtered, and washed three times with ethyl ether. The peptide was used without further purification. Analytical data were as follows: electrospray ionization mass spectrometry (ESI-MS): $(M+H)^+$ = 944; RP-HPLC: retention time (t_R) = 20.3 min and K′ = 4.8 (30%–80% MeCN; 30 min).

Selective Removal of Dde Protection Group. Cyclo(-Arg(Pbf)-Gly-Asp(OtBu)-D-3-iodo-Tyr-Lys(Dde)-) (0.2 mmol) was dissolved in 50 mL 2% hydrazine in dimethylformamide (DMF) and stirred for 30 min at ambient temperature. The solvent was removed in vacuo, and the residue was triturated with water. The precipitated peptide was isolated using a Varifuge 3.2S (Heraeus;

TABLE 1
Analytical Data of Cyclic Peptides*

No.	Peptide†	MW‡ (g/mol)	ESI-MS $(M + H)^+$	t_R (min)	K′	Log P§
P1	c(RGDyV)	590.64	591	13.0	4.9	
P2	c(RGD(l)yV)	716.53	717	21.2	8.6	−1.89
P3	c(RGDfY)	638.68	639	19.1	7.7	
P4	c(RGDf(l)Y)	764.58	765	24.7	10.2	−1.16
GP1	c(RGDyK(SAA))	850.88	851	9.1	3.1	
GP2	c(RGD(l)yK(SAA))	976.26	977	15.5	6.0	−2.45

*HPLC conditions: 10% MeCN with 0.1% TFA, 5 min; 10%–50% MeCN with 0.1% TFA, 30 min.
†Upper- and lowercase letters are used to distinguish between L- and D-amino acids in one-letter code for amino acids.
‡MW, molecular mass.
§Determined using ^{125}I-labeled derivatives.

Munich, Germany). Analytical data were as follows: ESI-MS, $(M+H)^+ = 1054$; RP-HPLC, $t_R = 14.1$ min and $K' = 4.4$ (30%–80% MeCN; 30 min).

Synthesis of Cyclo(-Arg(Mtr)-Gly-Asp(OtBu)-D-Tyr(tBu)-Lys-(SAA(Bn$_3$))-). Cyclo(-Arg(Mtr)-Gly-Asp(OtBu)-D-Tyr(tBu)-Lys-) (0.11 mmol) and 0.15 mmol of SAA(Bn$_3$) were dissolved in 7 mL DMF. To the combined solutions, two equivalents of 1-ethyl-3-(3′-dimethylaminopropyl)carbodiimide hydrochloride (EDCI × HCl) and two equivalents of HOBt were added. *N*-Ethylmorpholine was used to adjust the pH to approximately 7.5. After the solution was stirred for 12 h at ambient temperature, the solvent was reduced in vacuo, the residue was triturated with water, and the crude peptide was isolated by centrifugation. Analytical data were as follows: ESI-MS, $(M+H)^+ = 1445$; RP-HPLC, $t_R = 29.1$ min and $K' = 11.7$ (30%–100% MeCN; 30 min).

Synthesis of Cyclo(-Arg(Pbf)-Gly-Asp(OtBu)-D-3-Iodo-Tyr-Lys-(SAA)-). Cyclo(-Arg(Pbf)-Gly-Asp(OtBu)-D-3-iodo-Tyr-Lys-) (14 μmol) and 28 μmol SAA were dissolved in 1 mL DMF. After addition of 28 μmol of HOAt and 28 μmol of HATU, the pH was adjusted to pH 8 using diisopropylethylamine. The solution was allowed to stir for 70 h at ambient temperature. The solvent was reduced in vacuo, and the crude glycopeptide was precipitated with water and separated by centrifugation. Analytical data were as follows: ESI-MS, $(M+H)^+ = 1285$; RP-HPLC, $t_R = 17.5$ min; and $K' = 5.5$ (30%–80% MeCN; 30 min).

Removal of Side Chain Protection Groups of Peptides. Peptides were treated with 20 mL of a solution of 95% TFA, 2.5% water, and 2.5% triisobutylsilane for 24 h at ambient temperature. The mixture was filtered if necessary, evaporated in vacuo, triturated with ethyl ether, filtered again, and washed several times with ethyl ether.

Removal of Benzyl Groups of Cyclo(-Arg-Gly-Asp-D-Tyr-Lys-(SAA(Bn$_3$))-). The glycopeptide (47 μmol) was dissolved in 10 mL water/HOAc (1:1). After adding 50 mg 5% Pd on charcoal, the reaction mixture was stirred under hydrogen atmosphere at ambient temperature for 12 h. The catalyst was removed by filtration, and toluene was added before removing the solvent in vacuo. The crude product was freeze-dried. Analytical data were as follows: ESI-MS, $(M+H)^+ = 851$; RP-HPLC, $t_R = 9.1$ min; and $K' = 2.6$ (10%–50% MeCN; 30 min).

The crude cyclic peptides and glycopeptides were purified by RP-HPLC. Analytical data, including ^{1}H- and ^{13}C-chemical shift data for GP1, are given in Tables 1 and 2.

Radioiodination

The peptides cyclo(-Arg-Gly-Asp-D-Phe-Tyr-) P1 (*12*), cyclo(-Arg-Gly-Asp-D-Tyr-Val-) P3 (*12*), and cyclo(-Arg-Gly-Asp-D-

TABLE 2
^{1}H- and ^{13}C-Chemical Shift Data of GP1 in DMSO-d$_6$ at 300 K

Amino acid*†	^{1}H-shift						^{13}C-shift					
	H^N	$H^\alpha/H^{\alpha'}$	$H^\beta/H^{\beta'}$	$H^\gamma/H^{\gamma'}$	$H^\delta/H^{\delta'}$	Others	C^α	C^β	C^γ	C^δ	CO	Others
Arg^1	7.64	4.14	1.49/1.71	1.37	3.10	7.48 ($H^{N\epsilon}$)	51.8	28.3	25.3	40.2	171.1	156.6 (guanidino C)
Gly^2	8.30	3.22/4.02					43.2				169.4	
Asp^3	8.02	4.63	2.37/2.70				48.8	35.0			169.8	171.5 (COOH)
D-Tyr^4	7.89	4.37	2.69/2.81			6.62; 6.92 (aromatic Hs)	54.5	36.6			170.8	129.9; 114.6; 127.3 (aromatic Cs)
Lys^5	7.98	3.92	1.41/1.54	1.06	1.31	2.95 (H^ϵ), 7.75 ($H^{N\phi}$)	54.6	31.0	22.7	28.5	172.0	38.0 (C^ϵ)

*Sugar amino acid ^{1}H-shift data: H1, 3.56; H2, 3.62; H3, 3.31; H4, 3.18; H5, 3.10; H6, 3.67; H6′, 3.50; H^N, 7.66; and CO-CH_3, 1.76.
†Sugar amino acid ^{13}C-shift data: CO, 168.3; C1, 77.9; C2, 53.5; C3, 74.8; C4, 69.8; C5, 80.2; C6, 60.7; CO-CH_3, 169.4; CO-CH_3, 22.8.
Calibration was performed with reference to residual dimethyl sulfoxide signal (^{1}H, 2.49 ppm; ^{13}C, 39.5 ppm). Assignment of all proton and carbon resonances followed standard methods (*26*).

Tyr-Lys(SAA)-) GP1 were labeled with ^{125}I or ^{123}I (the last only for GP1) using the IODO-GEN method. The peptides (0.3–0.5 μmol) were dissolved in 200 μL of phosphate-buffered saline (PBS) (pH 7.4). The solutions were added to Eppendorf caps coated with 150 μg IODO-GEN and combined with 5–10 μL no-carrier-added (NCA) [^{125}I]NaI (30–80 MBq) or 25 μL carrier-added (CA) [^{123}I]NaI (185 MBq). After 30 min at ambient temperature, the solutions were removed from the solid oxidizing reagent. Purification was performed using RP-HPLC. Radiochemical purity was generally >95%. After removing the solvent in vacuo, the residue was triturated with water, passed through a C_{18} Sep-Pak column, washed two times with water (2 mL per time), and eluted with 2 mL methanol. The methanol was removed in vacuo, and the residue was dissolved with PBS (pH 7.4) to obtain solutions with an activity concentration of 370 kBq/100 μL that were ready for use in animal experiments. The overall radiochemical yield after RP-HPLC was ~50%.

Octanol/Water Partition Coefficient

About 5 kBq 3-[^{125}I]iodo-Tyr^5-cyclo(-Arg-Gly-Asp-D-Phe-Tyr-) ([^{125}I]P2) (*12*), 3-[^{125}I]iodo-D-Tyr^4-cyclo(-Arg-Gly-Asp-D-Tyr-Val-) ([^{125}I]P4) (*12*), or 3-[^{125}I]iodo-D-Tyr^4-cyclo(-Arg-Gly-Asp-D-Tyr-Lys(SAA)-) ([^{125}I]GP2) in 10 μL PBS dissolved in 490 μL PBS were added to 500 μL octanol in an Eppendorf tube. After the suspension was mixed for 3 min at room temperature, the caps were centrifuged (14,000 rpm for 6 min; Heraeus Biofuge 13; Heraeus, Hanau, Germany) and 100-μL aliquots of both layers were counted in a gamma counter.

Biological Assay

Purification of the proteins as well as the isolated integrin-binding assay have been described elsewhere (*12*). The inhibitory capacities of the cyclic peptides were quantified by measuring their effect on the interactions between immobilized integrin and biotinylated soluble ligands (vitronectin or fibrinogen). Recombinant human $\alpha_V\beta_3$ (*14*) and recombinant soluble human $\alpha_V\beta_5$ produced by similar procedures (*15*) were used in this study and gave identical results to the native placental integrins $\alpha_V\beta_3$ and $\alpha_V\beta_5$. The integrin preparations differed somewhat over time; thus the linear peptide Gly-Arg-Gly-Asp-Ser-Pro-Lys as well as the $\alpha_V\beta_3$-selective cyclo(-Arg-Gly-Asp-D-Phe-Val-) were used as internal standards to allow interassay comparability.

In Vivo Animal Experiments

Tumor Xenografts. Biodistribution of [^{125}I]P2 and [^{125}I]GP2 was evaluated in mice, using a murine osteosarcoma and a xenotransplanted human melanoma model. It has previously been demonstrated that both tumor models show high expression of the $\alpha_V\beta_3$ integrin (*12,16*).

Murine osteosarcomas induced by injection of ^{90}Sr were serially transplanted into BALB/c mice. Tumor pieces of ~1 mm^3 were injected by trocar close to the femur into the musculus quadriceps. Mice (20–25 g body weight) with tumor weights of ~500 mg were used for further investigations.

Human M21 melanoma cells (*16*) were cultured in a humidified atmosphere with 5% CO_2. The cell culture medium was RPMI 1640 (Seromed Biochrom, Berlin, Germany) supplemented with 10% fetal calf serum and gentamycine. Tumor xenografts were obtained by subcutaneous injection of 5×10^6 cells. Mice (20–25 g body weight) bearing tumors weighing 300–400 mg were used for biodistribution.

Biodistribution Studies. Nude mice bearing tumor xenografts of human melanoma M21 and BALB/c mice bearing murine osteosarcomas were injected intravenously with 300–400 kBq [^{125}I]P2, [^{125}I]P4, or [^{125}I]GP2. Injections into the tail vein were accomplished under short-time ether anesthesia.

The animals were killed and dissected at 10, 60, 120, and 240 min after injection of the ^{125}I-labeled peptides. Blood, plasma, liver, kidney, muscle, heart, brain, lung, spleen, intestine, thyroid, and tumor tissues were removed and weighed. The radioactivity in the tissues was measured using a gamma counter. Results are expressed as the percentage injected dose per gram of tissue (%ID/g). Each value represents the mean and SD of three or four animals.

Pretreatment Studies. Blocking of the $\alpha_V\beta_3$ integrin was performed by injecting cyclo(-Arg-Gly-Asp-D-Phe-Val-) at 3 mg/kg (before injection of [^{125}I]P2) or 6 mg/kg (before injection of [^{125}I]GP2) (*17,18*) at 10 min before injection of 300–400 kBq of the radioactive compound (approximately 8 ng/mouse) in 100 μL of PBS (pH 7.4). Animals were killed and dissected 60 min after injection of the ^{125}I-labeled peptides. Further processing was performed as described above.

Gamma-Camera Imaging. BALB/c mice bearing osteosarcomas were injected intravenously with 5.6 MBq [^{123}I]GP2. The animals were killed at 4 h after injection of the ^{123}I-labeled glycopeptide, and planar gamma-camera images were obtained (Siemens Multispect 3; Siemens Medical Systems, Hoffman Estates, IL). Acquisition time was 20 min/image.

RESULTS

In Vitro Binding Assay

The ability of cyclic pentapeptides to inhibit the binding of vitronectin and fibrinogen to the isolated immobilized $\alpha_{IIb}\beta_3$, $\alpha_V\beta_5$, and $\alpha_V\beta_3$ receptors was compared with that of the linear low-affinity peptide Gly-Arg-Gly-Asp-Ser-Pro-Lys and with the $\alpha_V\beta_3$-selective cyclo(-Arg-Gly-Asp-D-Phe-Val-) (*17,18*) as internal standards. The inhibitory peptides were able to fully suppress the binding of ligands to the isolated receptors, and the binding kinetics followed a classic sigmoid path. The inhibitory capacities (Table 3) of P2 were in the same range as the values found for cyclo(-Arg-Gly-Asp-D-Phe-Val-). P4 and the glycosylated derivatives GP1 and GP2 revealed two- to fourfold higher 50% inhibitory concentration (IC_{50}) values for all integrins. The selectivity of these peptides is comparable with the selectivity of cyclo(-Arg-Gly-Asp-D-Phe-Val-). The biological activities are ~100–150 times higher for the $\alpha_V\beta_3$ integrin than for $\alpha_V\beta_5$ or $\alpha_{IIb}\beta_3$. The negative control peptide cyclo(-Arg-D-Ala-Asp-Tyr-Val-) P5 showed no activity in the range of the test system for $\alpha_V\beta_3$ and $\alpha_{IIb}\beta_3$ ($\alpha_V\beta_5$ was not tested).

Biodistribution Studies

In the melanoma model, initial liver uptake of [^{125}I]GP2 was ~10-fold lower than that of [^{125}I]P2 (at 10 min postinjection, uptake was 22 ± 2.8 %ID/g for [^{125}I]P2 and 2.6 ± 0.2 %ID/g for [^{125}I]GP2) (for structures of the peptides, see Fig. 1). In contrast differences in renal tracer uptake were relatively small for the time points studied. The blood

TABLE 3
Inhibition of Vitronectin (Vn) Binding to Immobilized $\alpha_V\beta_3$ or $\alpha_V\beta_5$ and Fibrinogen (Fb) Binding to Immobilized $\alpha_{IIb}\beta_3$ ($n = 2$)

No.	Peptide*	$IC_{50}(\alpha_{IIb}\beta_3$; Fb) (nmol/L)	$IC_{50}(\alpha_V\beta_5$; Vn) (nmol/L)	$IC_{50}(\alpha_V\beta_3$; Vn) (nmol/L)
	GRGDSPK	1,000	>10,000	600
	c(RGDfV)	1,000	1,000	7
P2	c(RGD(l)yV)	700	600	10
P4	c(RGDf(l)Y)	3,000	4,000	40
GP1	c(RGDyK(SAA))	3,000	4,000	20
GP2	c(RGD(l)yK(SAA))	5,000	2,000	40
P5	c(RaDYV)	NA†		NA†

*Upper- and lowercase letters are used to distinguish between L- and D-amino acids in one-letter code for amino acids.
†NA, compound shows no activity in test system.

clearance of [^{125}I]P2 was approximately threefold faster than that for [^{125}I]GP2 (area under the blood time–activity curve (39 %ID/min g^{-1} for [^{125}I]P2 vs. 109 %ID/min g^{-1} for [^{125}I]GP2). Tumor uptake of [^{125}I]GP2 was higher than that for [^{125}I]P2 at all time points. At 240 min after tracer injection, tumor uptake of [^{125}I]GP2 was 1.7 ± 0.5 %ID/g, whereas it was only 0.4 ± 0.2 %ID/g for [^{125}I]P2. At this time point, the tumor-to-blood ratio (T/B) was slightly higher for [^{125}I]GP2 than for [^{125}I]P2 (8.9 vs. 6.8, respectively). At 240 min postinjection, the activity concentration within the thyroid was 0.3 ± 0.1 %ID/g for [^{125}I]P2 and 11.8 ± 6.5 %ID/g for [^{125}I]GP2. All other organ systems except the intestine showed only low uptake of [^{125}I]P2 and [^{125}I]GP2. However, the activity concentration in these organs (e.g., muscle, heart, and lung) was about twofold higher for [^{125}I]GP2 than for [^{125}I]P2. The tumor-to-muscle ratio (T/M) at 240 min postinjection was 4.1 for [^{125}I]P2 and 7.0 for [^{125}I]GP2.

Similar results were obtained for the osteosarcoma model. Again, tumor uptake of [^{125}I]GP2 was higher than that of [^{125}I]P2 at all time points. At 240 min postinjection, tumor uptake of [^{125}I]GP2 was 3.4-fold higher than that of [^{125}I]P2 (3.1 ± 0.3 %ID/g vs. 0.9 ± 0.2 %ID/g). At this time point, the T/B was 16.0 for [^{125}I]GP2, whereas it was only 7.7 for [^{125}I]P2. For both tracers, the radioactivity concentration in the thyroid was considerably higher than that for the melanoma (nude mouse) model ([^{125}I]P2: 30 ± 11 %ID/g; [^{125}I]GP2: 175 ± 34 %ID/g). For all other organ systems, trends in tracer uptake of [^{125}I]P2 and [^{125}I]GP2 similar to those in the melanoma model were observed.

Peptide [^{125}I]P4 was examined using BALB/c mice bearing osteosarcomas. Sixty minutes postinjection of [^{125}I]P4, most of the administered activity (about 75 %ID/mouse) was detected in the intestine. All other examined organs showed only small amounts of the administered activity (*12*).

Details of the tissue distribution of [^{125}I]P2 and [^{125}I]GP2 are summarized in Table 4 and Figure 2. The thyroid uptake showed some variance. This variance may have resulted from variable small amounts of free iodine in the different

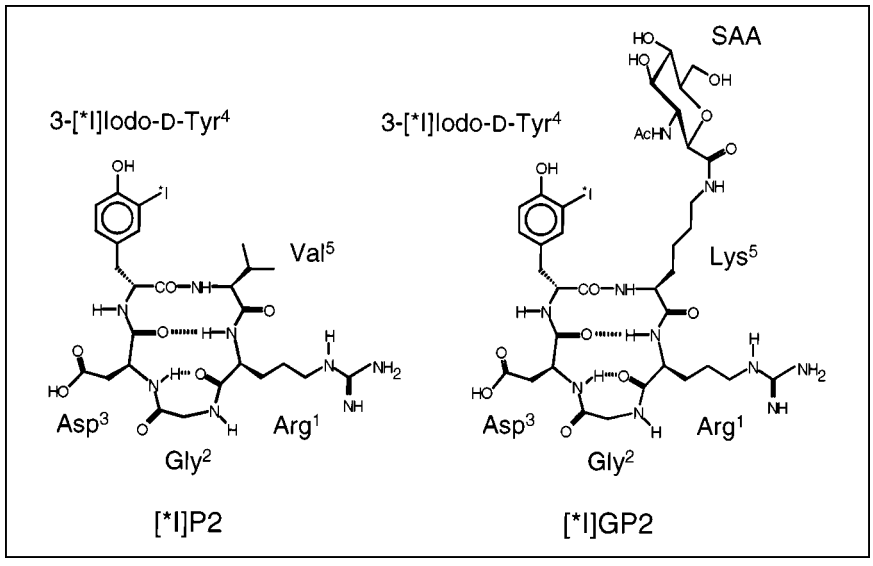

FIGURE 1. Schematic structure of first generation tracer [^{125}I]P2 and new glycosylated tracer [^{125}I]GP2. Both peptides show characteristic βII′-turn with D-Tyr in i + 1 position and RGD site in γ-turn conformation responsible for $\alpha_V\beta_3$ selectivity.

TABLE 4
Biodistribution Data for [^{125}I]P2 and [^{125}I]GP2 in Melanoma-Bearing Nude Mice and Osteosarcoma-Bearing BALB/c Mice

Organ time after injection (min)	[^{125}I]P2 (n = 3)		[^{125}I]GP2 (n = 4)	
	Melanoma	Osteosarcoma	Melanoma	Osteosarcoma
Blood				
10	0.77 ± 0.02	1.72 ± 0.44	2.20 ± 0.11	3.59 ± 0.35
60	0.17 ± 0.02	0.27 ± 0.03	0.41 ± 0.11	0.68 ± 0.25
120		0.17 ± 0.01	0.23 ± 0.08	0.60 ± 0.01
240	0.06 ± 0.02	0.12 ± 0.02	0.19 ± 0.09	0.19 ± 0.04
Serum				
10	1.43 ± 0.01	3.04 ± 0.82	3.64 ± 0.18	6.36 ± 0.68
60	0.29 ± 0.03	0.43 ± 0.06	0.57 ± 0.15	1.00 ± 0.40
120		0.30 ± 0.02	0.32 ± 0.10	1.03 ± 0.07
240	0.09 ± 0.03	0.21 ± 0.04	0.24 ± 0.10	0.24 ± 0.06
Liver				
10	21.96 ± 2.78	19.06 ± 0.92	2.59 ± 0.24	6.03 ± 0.53
60	11.23 ± 1.95	10.36 ± 2.27	1.22 ± 0.32	2.98 ± 0.98
120		4.22 ± 1.91	0.72 ± 0.19	2.04 ± 0.11
240	0.78 ± 0.28	2.18 ± 0.65	0.56 ± 0.18	1.23 ± 0.19
Kidneys				
10	12.09*	10.94 ± 2.37	6.38 ± 0.31	14.03 ± 1.63
60	3.30 ± 0.12	2.64 ± 0.35	2.23 ± 0.43	5.01 ± 1.52
120		2.10 ± 0.23	1.62 ± 0.34	3.40 ± 0.51
240	0.28 ± 0.16	1.08 ± 0.18	1.30 ± 0.48	4.10 ± 0.67
Muscle				
10	0.42 ± 0.04	0.94 ± 0.13	0.84 ± 0.05	1.75 ± 0.73
60	0.25 ± 0.05	0.43 ± 0.05	0.50 ± 0.19	0.68 ± 0.17
120		0.36 ± 0.02	0.29 ± 0.03	0.54 ± 0.11
240	0.10 ± 0.03	0.24 ± 0.04	0.23 ± 0.07	0.53 ± 0.05
Tumor				
10	2.07 ± 0.32	3.50 ± 0.49	2.71 ± 0.18	5.86 ± 1.19
60	1.30 ± 0.13	2.02 ± 0.49	2.05 ± 0.55	2.58 ± 0.91
120		1.46 ± 0.16	1.81 ± 0.30	2.45 ± 0.39
240	0.41 ± 0.15	0.92 ± 0.16	1.69 ± 0.54	3.05 ± 0.31
Heart				
10	0.60 ± 0.07	1.87 ± 0.35	1.31 ± 0.03	2.87 ± 0.25
60	0.22 ± 0.07	0.67 ± 0.13	0.46 ± 0.10	1.19 ± 0.34
120		0.49 ± 0.03	0.35 ± 0.08	0.91 ± 0.18
240	0.07 ± 0.02	0.24 ± 0.04	0.27 ± 0.06	0.70 ± 0.10
Brain				
10	0.09 ± 0.02		0.17 ± 0.02	0.20 ± 0.01
60	0.05 ± 0.01		0.07 ± 0.01	0.09 ± 0.02
120			0.05 ± 0.01	0.09 ± 0.03
240	0.02 ± 0.01		0.05 ± 0.01	0.11 ± 0.06
Lung				
10	2.36 ± 0.46	4.58 ± 1.05	3.91 ± 0.35	7.02 ± 0.91
60	0.93 ± 0.21	1.68 ± 0.18	1.51 ± 0.40	2.51 ± 0.73
120		1.06 ± 0.11	0.98 ± 0.21	1.72 ± 0.21
240	0.29 ± 0.10	0.55 ± 0.05	0.83 ± 0.20	1.49 ± 0.16
Spleen				
10	1.41 ± 0.36		2.25 ± 0.11	3.97 ± 0.22
60	0.78 ± 0.26		1.23 ± 0.32	2.47 ± 0.72
120			0.99 ± 0.24	1.83 ± 0.18
240	0.10 ± 0.04		0.79 ± 0.30	1.52 ± 0.22
Intestine				
10		4.31 ± 0.18	2.21 ± 0.20	4.41 ± 0.21
60		12.83 ± 1.74	2.61 ± 0.61	3.97 ± 1.32
120		15.04 ± 2.51	2.16 ± 0.41	4.33 ± 0.38
240		20.05 ± 3.40	2.92 ± 0.63	4.93 ± 1.04
Thyroid				
10	2.21 ± 0.64	3.49 ± 2.27	8.80 ± 3.29	16.96 ± 4.29
60	1.95 ± 0.46	6.40 ± 2.27	7.69 ± 2.54	47.81 ± 39.42
120		15.61 ± 7.08	14.32 ± 5.21	87.59 ± 44.09
240	0.29 ± 0.08	30.02 ± 11.16	11.82 ± 6.54	174.63 ± 33.71

* Experiments gave only one data point.
Values are given as %ID/g ± SD.

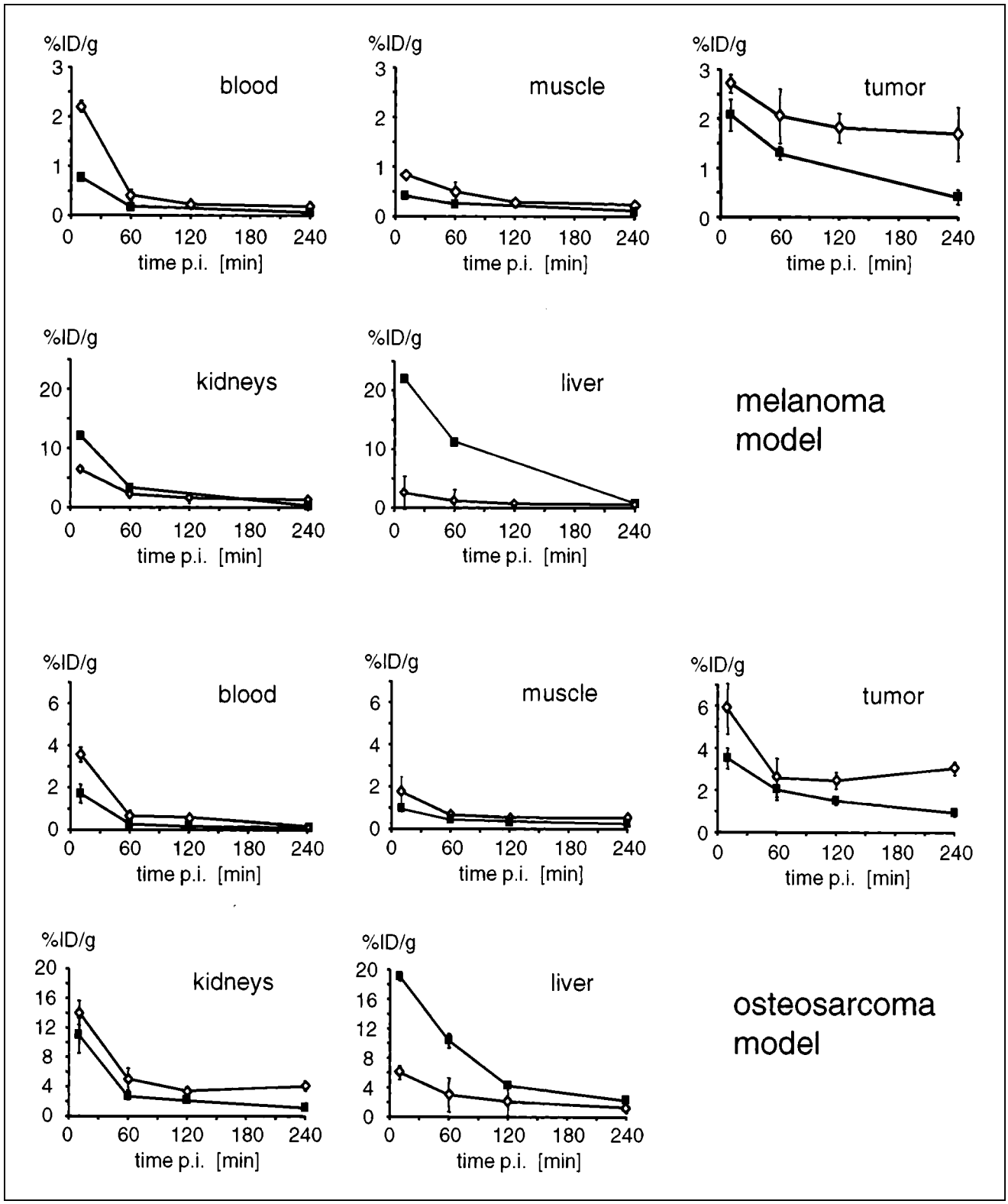

FIGURE 2. Comparison of biodistribution data of [^{125}I]P2 (■) and [^{125}I]GP2 (◇) in melanoma-bearing nude mice and in BALB/c mice with osteosarcoma. Error bars denote SD. For some data points, error bars are not visible, because SD was smaller than size of symbol. p.i. = postinjection.

preparations used for the biodistribution studies (radiochemical purity is generally >95%). However, because of the low mass of the thyroid, the absolute uptake in this organ was still low and did not interfere with the quality of the image (e.g., 200 %ID/g thyroid corresponded with ~0.5% ID per mouse). This was also confirmed by gamma-camera imaging.

Pretreatment Studies

The results of the pretreatment studies of [^{125}I]P2 and [^{125}I]GP2 using the melanoma/mouse model are shown in Figure 3. Blocking with 3 mg cyclo(-Arg-Gly-Asp-D-Phe-Val-)/kg for 10 min before the injection of [^{125}I]P2 and with 6 mg cyclo(-Arg-Gly-Asp-D-Phe-Val-) for 10 min before the injection of [^{125}I]GP2, respectively, reduced the activity accumulation in the tumor to ~0.5 %ID/g at 60 min postinjection for both tracers. This corresponds to a tracer accumulation of ~40% of control for [^{125}I]P2 and of ~15% of control for [^{125}I]GP2.

Gamma-Camera Imaging

The planar image at 4 h postinjection of [^{123}I]GP2 (Fig. 4) clearly shows a contrasting tumor on the left flank of the mouse with only marginal background signal. High-activity concentrations also were found in the intestine and in the unblocked thyroid.

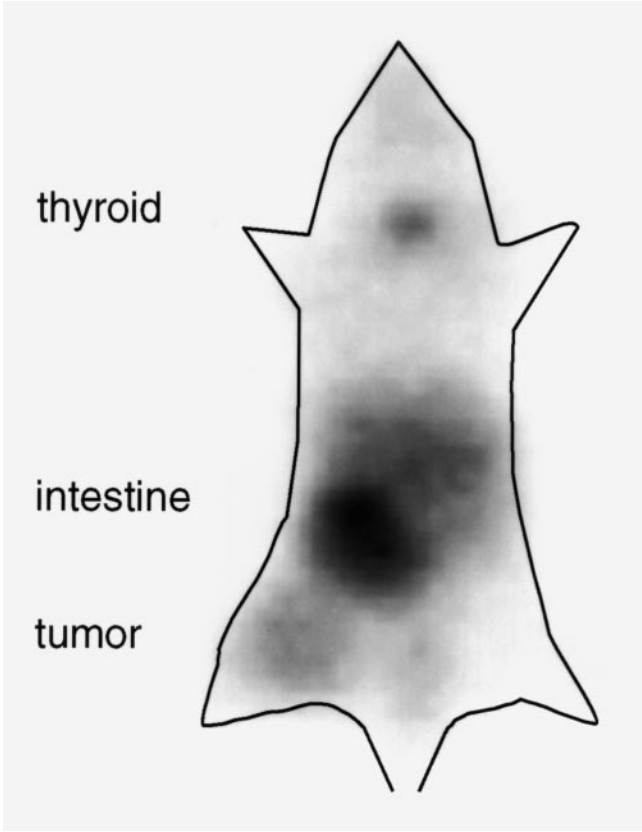

FIGURE 4. Gamma-camera image 240 min after intravenous injection of 555 kBq [^{125}I]GP2 of osteosarcoma-bearing BALB/c mouse. Contrasting tumor is clearly shown on left flank. Only additional higher activity concentration was found in intestine and in thyroid.

DISCUSSION

Sugar moieties are hydrophilic compounds that can be used to improve different properties of biologically active peptides, such as bioavailability (*19*,*20*), resistance against proteases (*21*), solubility under physiological conditions (*22*), or penetration of the brain–blood barrier (*23*). For example, Schottelius et al. (*24*) used different sugar moieties, like glucose and mannose, to modify the pharmacokinetics and tumor accumulation of SSTR-agonists. The results included reduced liver uptake and elevated tumor uptake, leading to excellent tumor-to-organ ratios. The use of sugar amino acids for the improvement of these properties offers some advantages. These amino acids can easily be used with standard peptide synthesis protocols and, because of the C—C bond at the anomeric center, the resulting C-glycosylated peptides are very stable against metabolic degradation.

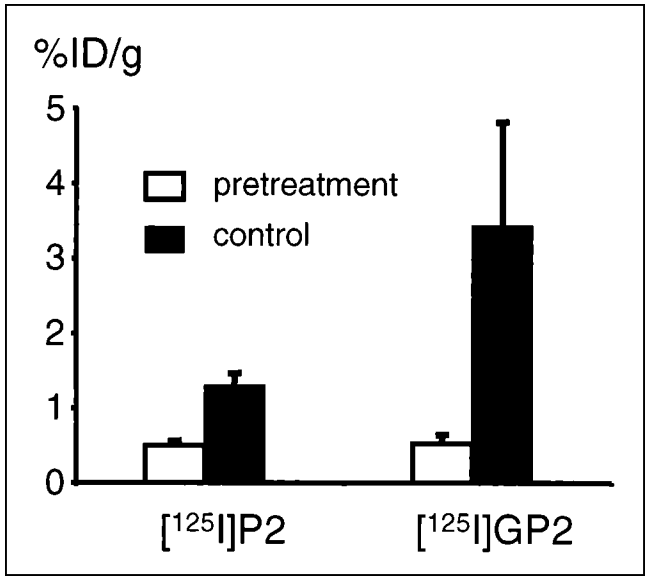

FIGURE 3. Activity accumulation in tumor after pretreatment using $\alpha_V\beta_3$-selective peptide cyclo(-Arg-Gly-Asp-D-Phe-Val-) in melanoma-bearing nude mice (n = 3). Data were determined 60 min after injection of [^{125}I]P2 or [^{125}I]GP2. Cyclo(-Arg-Gly-Asp-D-Phe-Val-) was injected 10 min before tracer injection. Right columns show activity accumulation 60 min after injection of tracer as control.

In this report, we have described the introduction of a sugar amino acid to improve the pharmacokinetics of our recently described radiolabeled RGD-containing pentapeptides (*12*). We have also demonstrated that the optimized glycosylated tracer allows for high-quality gamma-camera imaging of $\alpha_V\beta_3$-expressing tumors in mice. These data suggest that this tracer could be a helpful tool for planning and monitoring of antiangiogenic therapies.

Our comprehensive investigations concerning the development of integrin subtype-selective cyclic peptides re-

sulted, about 8 y ago, in the first selective $\alpha_V\beta_3$-antagonist cyclo(-Arg-Gly-Asp-D-Phe-Val-) (*17,18,25*). This cyclic pentapeptide was the lead structure for the development of all further compounds. Therefore, the design of the glycosylated second-generation tracer was also based on this structure and on data from further structure activity investigations (*26*), which demonstrated that substitution of the amino acid adjacent to the arginine residue in the cyclic pentapeptide core had no influence on selectivity and affinity for $\alpha_V\beta_3$. Thus, valine of P2 was substituted with lysine, allowing the conjugation of the lysine side chain amino group with the carboxy function of the sugar amino acid (Fig. 1). Comparison of the ^{1}H- and ^{13}C-chemical-shift data of GP1 (Table 2) with a set of cyclic pentapeptides with the same core structure cyclo(-Arg-Gly-Asp-D-Xxx-Yyy-) (*26*) indicates that the conjugation of the sugar moiety had no influence on the bent conformation of the RGD-side, which is important for high $\alpha_V\beta_3$ affinity and selectivity.

The results of the isolated, immobilized integrin receptor-binding assay confirmed that introduction of the sugar moiety at the amino function of Lys^5 has only minor influence on the $\alpha_V\beta_3$ affinity and selectivity. The glycosylated peptide GP1 revealed about twofold higher IC_{50} values and similar selectivities for $\alpha_V\beta_3$ compared with the lead structure cyclo(-Arg-Gly-Asp-D-Phe-Val) (*17*). Subsequent iodination of GP1 led to a marginal reduction in affinity and selectivity.

Recently, it has been shown that $\alpha_V\beta_5$ also seems to be involved in angiogenesis processes. Friedlander et al. (*7*) demonstrated that the induction of angiogenesis in the chicken egg (chick choreoallantoic membrane model) with different cytokines follows different pathways. Stimulation by basic fibroblast growth factor or by tumor necrosis factor α seems to induce $\alpha_V\beta_3$ expression, whereas vascular endothelial growth factor, transforming growth factor α, or phorbol ester stimulates expression of the $\alpha_V\beta_5$ integrin. In the study by Friedlander et al. (*7*), cyclo(-Arg-Gly-Asp-D-Phe-Val-), developed by Kessler et al. (*17,18*), blocked angiogenesis regardless of the stimulated pathway. Thus, the described tracers should allow monitoring of tumor-induced angiogenesis that is independent of the α_V integrin involved. However, in our in vitro assay, neither cyclo (-Arg-Gly-Asp-D-Phe-Val-) nor the derivatives described here showed high affinity for $\alpha_V\beta_5$. This different behavior in vitro and in vivo will be examined in further experiments.

The receptor-specific accumulation of [^{125}I]GP2 in vivo was demonstrated by competition experiments using cyclo (-Arg-Gly-Asp-D-Phe-Val-) (Fig. 2). Pretreatment of the mice with the cold peptide clearly reduced the activity accumulation in the tumor. Despite the different amounts of cyclo(-Arg-Gly-Asp-D-Phe-Val-) used ([^{125}I]GP2, 6 mg/kg; [^{125}I]P2, 3 mg/kg), ~0.5 %ID/g at 60 min postinjection could be found in tumors in both pretreatment experiments, perhaps reflecting the amount of unspecific bound activity. This result has been confirmed by investigations with the nonspecific control peptide [^{125}I]-3-iodo-Tyr^4-cyclo(-Arg-D-Ala-Asp-Tyr-Val-), which revealed an activity uptake of 0.32 %ID/g at 60 min postinjection in the tumor (*12*). These results indicate that [I]GP2 may in fact be used to document blockade of the $\alpha_v\beta_3$ integrin during therapy with unlabeled antagonists such as EMD121974 (*27*), SC68448 (*28*), and SM256 (*29*).

Comparison of the biodistribution data of the first-generation tracer [^{125}I]P2 with the glycosylated second-generation peptide [^{125}I]GP2 (Fig. 2) showed that [^{125}I]P2 preferred the hepatobiliary elimination pathway and [^{125}I]GP2 the renal elimination pathway. [^{125}I]P4, the other first-generation tracer, revealed even faster elimination kinetics than those of [^{125}I]P2, with most of the administered activity found in the intestine at 60 min postinjection. This result indicates that the more hydrophobic [^{125}I]P2 and [^{125}I]P4 were eliminated rapidly from the circulatory system, whereas the hydropilic [^{125}I]GP2 (see also logP values in Table 1) was able to remain slightly longer in the circulatory system, which resulted in a clear increase in tracer uptake in the tumor for the glycosylated tracer. The slower blood clearance of [^{125}I]GP2 may also explain the higher activity concentration found in muscle, myocardium, and lung tissue. Nevertheless, introduction of a hydrophilic group had beneficial effects on the pharmacokinetics and markedly improved the uptake of the tracer in the $\alpha_V\beta_3$-expressing tumors. In addition, the uptake of the glycosylated tracer in both tumor models seemed to remain very constant between 60 and 240 min postinjection. This suggests that [I]GP2 is suitable for SPECT imaging when constant levels of tracer concentrations during data acquisition are important for high-quality images.

The improved pharmacokinetics and increased uptake of [^{125}I]GP2 in the tumor resulted in increased T/Bs and T/Ms (*30,31*). The gamma-camera image of an osteosarcoma-bearing mouse at 240 min after injection of [^{123}I]GP2 confirmed the good tumor-to-organ ratios. The uptake in the thyroid was somewhat higher than that for [^{125}I]P2, but even this value reflected a low accumulation in the whole thyroid (0.4 %ID for a thyroid weight of 2 mg). This indicated, in addition to the low signal of the thyroid visible at the gamma-camera image, that [*I]GP2 is also sufficiently stable towards deiodination in vivo.

A linear decapeptide containing two RGD sites has already been used for imaging in one patient study (*32*). In 14 patients with melanoma, 11 metastatic lesions were imaged with positive contrast. However, background activity in the lung and abdomen was high. Furthermore, the affinity of the peptide for different integrins with an RGD-binding site such as $\alpha_V\beta_3$, $\alpha_V\beta_5$, and $\alpha_{IIb}\beta_3$ has not been described. On the other hand, it has been shown that small linear peptides show only low selectivity for distinct integrin subtypes, recognizing the RGD sequence (e.g., GRGDSPK (*33*)). Thus, in contrast to images obtained by [I]GP2, which provide information regarding $\alpha_V\beta_3$ expression, it is unclear at the moment which biological signal is determined by this linear decapeptide.

In animal studies, visualization of $\alpha_V\beta_3$ expression has been reported by anti $\alpha_V\beta_3$ antibody (LM609)-coated paramagnetic liposomes and MRI (*34*). An important advantage of this approach is the high spatial resolution achieved, which may allow us to image small angiogenic hot spots within a tumor mass. However, the long plasma half-life of the liposomes hampers differentiation of intravascular and specifically bound liposomes. In addition, quantification of $\alpha_V\beta_3$ expression is expected to be limited by the nonlinear relationship between changes in the MRI signal and the concentration of antibody-coated liposomes in the tissue. Furthermore, it is not clear whether blockade of $\alpha_v\beta_3$ by small peptide antagonists can be determined using the LM609 antibody.

In contrast to antibody-coated liposomes, the glycosylated cyclic RGD-peptide [I]GP2 showed rapid tumor uptake and blood clearance, resulting in good T/Bs as early as 60 min after tracer injection. Thus, the biokinetic properties of these compounds are compatible with gamma-camera imaging and SPECT studies using short-lived radiopharmaceuticals such as ^{123}I. Moreover, labeling with ^{18}F for PET is also possible. Most recently, we developed ^{99m}Tc-, ^{188}Re-, and ^{90}Y-labeled RGD peptides for SPECT imaging and endoradiotherapeutic use (*35*) and the first ^{18}F-labeled tracer based on this glycopeptide (*36*), which showed promising results in the preliminary studies.

In clinical studies, radiolabeled RGD-peptides may be used for several applications. Imaging may be applied to document $\alpha_V\beta_3$ expression in tumor before administration of $\alpha_V\beta_3$ antagonists. This would allow appropriate selection of patients entering a clinical trial. Furthermore, radiolabeled RGD-peptides may be used to assess the inhibition of the $\alpha_V\beta_3$ integrin by antagonists. Thus, the optimum dosage for treatment with these drugs may be determined. Finally, uptake of RGD-peptides may be a measure for angiogenic activity, because $\alpha_V\beta_3$ is expressed on activated but not on quiescent endothelial cells (*37*). This class of tracer may also allow monitoring of the effects of other forms of antiangiogenic therapy. However, $\alpha_V\beta_3$ expression has also been documented in various tumor cells lines (*38*). Therefore, future studies are required to determine whether the signal obtained in vivo is specific for angiogenic activity. Nevertheless, common pathways link the processes leading to the formation and penetration of newly formed vessels during tumor-induced angiogenesis and tumor invasiveness. A cascade of enzymatic pathways leads to the alterations of the extracellular matrix that permit neovascularization and tumor invasiveness (*39*). Numerous experimental studies have suggested that $\alpha_V\beta_3$ plays a pivotal role in both processes (*1,2*). Recent clinical studies support these experimental data by showing a significant correlation between $\alpha_V\beta_3$ expression and patient survival (*40*). Therefore, imaging of $\alpha_V\beta_3$ expression in patients may provide unique means to characterize the biological aggressiveness of a malignant tumor in an individual patient.

CONCLUSION

The glycosylated second-generation tracer [I]GP2 exhibits high affinity for the $\alpha_V\beta_3$ integrin in vitro and specific binding to $\alpha_V\beta_3$-expressing tumors in vivo. This study demonstrated that our concept of introducing a sugar moiety in a peptidic tracer resulted in an increased initial activity concentration in the blood and drastically reduced uptake in the liver, leading to a clearly improved activity accumulation in the tumor. Thus, this glycosylated tracer allows noninvasive visualization of the $\alpha_V\beta_3$ status with SPECT, which should enable specific therapeutic planning and control of antiangiogenetic therapies. Furthermore, this optimized radiolabeled $\alpha_V\beta_3$ antagonist is a lead structure for further developments to generate new tracers for the quantification of $\alpha_V\beta_3$ expression using PET.

ACKNOWLEDGMENTS

This work was supported by a grant from the Sander-Stiftung (grant no. 96.017.2). We thank Kai Borchers, Wolfgang Linke, Susanne Daum, Friederike Rau, and Katrin Fischer for excellent technical assistance; Gabi Michalke, Peter Nieland, and Annemarie Aigner for preparing the gamma-camera images; Burghard Cordes for conducting the mass spectral analyses; and Jodi Neverve for carefully reading the manuscript. Parts of the study were presented in 1997 at the 12th International Symposium on Radiopharmaceutical Chemistry in Uppsala, Sweden, and the 1999 Annual Meeting of the German Society of Nuclear Medicine in Ulm.

REFERENCES

1. Clezardin P. Recent insights into the role of integrins in cancer metastasis. *Cell Mol Life Sci.* 1998;54:541–548.
2. Eliceiri BP, Cheresh DA. The role of α_v integrins during angiogenesis: insights into potential mechanisms of action and clinical development. *J Clin Invest.* 1999;103:1227–1230.
3. Cox D, Aoki T, Seki j, Motoyama Y, Yoshida K. The pharmacology of integrins. *Med Res Rev.* 1994;14:192–228.
4. Hynes RO. Integrins: versatility, modulation, and signaling in cell adhesion. *Cell.* 1992;69:11–25.
5. Stromblad S, Cheresh DA. Integrins, angiogenesis and vascular cell survival. *Chem Biol.* 1996;3:881–885.
6. Felding-Habermann B, Mueller BM, Romerdahl CA, Cheresh DA. Involvement of integrin α_v gene expression in human melanoma tumorigenicity. *J Clin Invest.* 1992;89:2018–2022.
7. Friedlander M, Brooks PC, Shaffer RW, Kincaid CM, Varner JA, Cheresh DA. Definition of two angiogenic pathways by distinct α_v integrins. *Science.* 1995; 270:1500–1502.
8. Brooks PC, Montgomery AM, Rosenfeld M, et al. Integrin $\alpha_v\beta_3$ antagonists promote tumor regression by inducing apoptosis of angiogenic blood vessels. *Cell.* 1994;79:1157–1164.
9. Brooks PC, Clark RA, Cheresh DA. Requirement of vascular integrin $\alpha_v\beta_3$ for angiogenesis. *Science.* 1994;264:569–571.
10. Brooks PC, Stromblad S, Klemke R, Visscher D, Sarkar FH, Cheresh DA. Antiintegrin $\alpha_v\beta_3$ blocks human breast cancer growth and angiogenesis in human skin. *J Clin Invest.* 1995;96:1815–1822.
11. Brower V. Tumor angiogenesis—new drugs on the block. *Nat Biotechnol.* 1999;17:963–968.

12. Haubner R, Wester HJ, Reuning U, et al. Radiolabeled $\alpha_v\beta_3$ integrin antagonists: a new class of tracers for tumor targeting. *J Nucl Med.* 1999;40:1061–1071.
13. Hoffmann M, Burkhart F, Hessler G, Kessler H. C-glycosid analogues of N4-(2-acetamido-2-deoxy-β-D-glucopyranosyl)-l-asparagine: synthesis and conformational analysis of a cyclic C-glycopeptide. *Helv Chim Acta.* 1996;79:1519–1532.
14. Mehta RJ, Diefenbach B, Brown A, et al. Transmembrane-truncated $\alpha_v\beta_3$ integrin retains high affinity for ligand binding: evidence for an 'inside-out' suppressor? *Biochem J.* 1998;330:861–869.
15. Kraft S, Diefenbach B, Mehta RJ, Jonczyk A, Luckenbach GA, Goodman SL. Definition of an unexpected ligand recognition motif for $\alpha_v\beta_6$ integrin. *J Biol Chem.* 1999;274:1979–1985.
16. Cheresh DA, Spiro RC. Biosynthetic and functional properties of an Arg-Gly-Asp-directed receptor involved in human melanoma cell attachment to vitronectin, fibrinogen, and von Willebrand factor. *J Biol Chem.* 1987;262:17703–17711.
17. Aumailley M, Gurrath M, Müller G, Calvete J, Timpl R, Kessler H. Arg-Gly-Asp constrained within cyclic pentapeptides: strong and selective inhibitors of cell adhesion to vitronectin and laminin fragment P1. *FEBS Lett.* 1991;291:50–54.
18. Pfaff M, Tangemann K, Müller B, et al. Selective recognition of cyclic RGD peptides of NMR defined conformation by $\alpha_{IIb}\beta_3$, $\alpha_v\beta_3$, and $\alpha_5\beta_1$ integrins. *J Biol Chem.* 1994;269:20233–20238.
19. Kihlberg J, Ahman J, Walse B, et al. Glycosylated peptide hormones: pharmacological properties and conformational studies of analogues of [1-desamino,8-D-arginine]vasopressin. *J Med Chem.* 1995;38:161–169.
20. Albert R, Marbach P, Bauer W, et al. SDZ CO 611:a highly potent glycated analog of somatostatin with improved oral activity. *Life Sci.* 1993;53:517–525.
21. Marastoni M, Spisani S, Tomatis R. Synthesis and biological activity of D-glycopyranosyl peptide T derivatives. *Arzneimittelforschung/Drug Res.* 1994;44:984–987
22. Michael K, Wittmann V, König W, Sandow J, Kessler H. S- and C-glycopeptide derivatives of an LH-RH agonist. *Int J Peptide Protein Res.* 1996;48:59–70.
23. Polt R, Porreca F, Szabo LZ, et al. Glycopeptide enkephalin analogues produce analgesia in mice: evidence for penetration of the blood-brain barrier. *Proc Natl Acad Sci USA.* 1994;91:7114–7118.
24. Schottelius M, Senekowitsch-Schmidtke R, Scheidhauer K, Kessler H, Schwaiger M, Wester HJ. Glycation of radioiodinated octreotates increase renal excretion and tumor uptake [abstract]. *Nucl Med Commun.* 2000;21:579.
25. Gurrath M, Müller G, Kessler H, Aumailley M, Timpl R. Conformation/activity studies of rationally designed potent anti-adhesive RGD peptides. *Eur J Biochem.* 1992;210:911–921.
26. Haubner R, Gratias R, Diefenbach B, Goodman SL, Jonczyk A, Kessler H. Structural and functional aspects of RGD-containing cyclic pentapeptides as highly potent and selective integrin $\alpha_v\beta_3$ antagonists. *J Am Chem Soc.* 1996;118:7461–7472.
27. Dechantsreiter MA, Planker E, Mathä B, et al. N-methylated cyclic RGD peptides as highly active and selective $\alpha_v\beta_3$ integrin antagonists. *J Med Chem.* 1999;42:3033–3040.
28. Carron CP, Meyer DM, Pegg JA, et al. A peptidomimetic antagonist of the integrin $\alpha_v\beta_3$ inhibits Leydig cell tumor growth and the development of hypercalcemia of malignancy. *Cancer Res.* 1998;58:1930–1935.
29. Kerr JS, Wexler RS, Mousa SA, et al. Novel small molecule α_v integrin antagonists: comparative anti-cancer efficacy with known angiogenesis inhibitors. *Anticancer Res.* 1999;19:959–968.
30. Haubner R, Wester HJ, Senekowitsch-Schmidtke R, et al. RGD-peptides for tumor targeting: biological evaluation of radioiodinated analogs and introduction of a novel glycosylated peptide with improved biokinetics [abstract]. *J Lab Compd Radiopharm.* 1997;40:383–385.
31. Haubner R, Wester HJ, Senekowitsch-Schmidtke R, et al. Glycosylated RGD-peptides for the monitoring of the $\alpha_v\beta_3$ integrin expression [in German] [abstract]. *Nuklearmedizinischen.* 1999;38:A23.
32. Sivolapenko GB, Skarlos D, Pectasides D, et al. Imaging of metastatic melanoma utilising a technetium-99m labelled RGD-containing synthetic peptide. *Eur J Nucl Med.* 1998;25:1383–1389.
33. Fauchere JL, Morris AD, Thurieau C, Simonet S, Verbeuren TJ, Kieffer N. Modulation of the activity and assessment of the receptor selectivity in a series of new RGD-containing peptides. *Int J Pept Protein Res.* 1993;42:440–444.
34. Sipkins DA, Cheresh DA, Kazemi MR, Nevin LM, Bednarski MD, Li KC. Detection of tumor angiogenesis in vivo by $\alpha_v\beta_3$-targeted magnetic resonance imaging. *Nat Med.* 1998;4:623–626.
35. Bock M, Bruchertseifer F, Haubner R, et al. Tc-99m-, Re-188- and Y-90-labeled $\alpha_v\beta_3$ antagonists: promising tracer for tumor-induced angiogenesis [abstract]. *J Nucl Med.* 2000;41(suppl):41P.
36. Haubner R, Wester HJ, Mang C, Senekowitsch-Schmidtke R, Kessler H, Schwaiger M. Synthesis and first evaluation of a [^{18}F]SAA-labeled RGD-peptide for monitoring the $\alpha_v\beta_3$ integrin expression [abstract]. *J Nucl Med.* 2000;41(suppl):42P.
37. Gasparini G. The rationale and future potential of angiogenesis inhibitors in neoplasia. *Drugs.* 1999;58:17–38.
38. Marshall JF, Hart IR. The role of α_v-integrins in tumour progression and metastasis. *Semin Cancer Biol.* 1996;7:129–138.
39. Stetler-Stevenson WG, Corcoran ML. Tumor angiogenesis: functional similarities with tumor invasion. *EXS.* 1997;79:413–418.
40. Gasparini G, Brooks PC, Biganzoli E, et al. Vascular integrin $\alpha_v\beta_3$: a new prognostic indicator in breast cancer. *Clin Cancer Res.* 1998;4:2625–2634.

JNM The Journal of NUCLEAR MEDICINE

Glycosylated RGD-Containing Peptides: Tracer for Tumor Targeting and Angiogenesis Imaging with Improved Biokinetics

Roland Haubner, Hans-Jürgen Wester, Fred Burkhart, Reingard Senekowitsch-Schmidtke, Wolfgang Weber, Simon L. Goodman, Horst Kessler and Markus Schwaiger

J Nucl Med. 2001;42:326-336.

The Journal of Nuclear Medicine is published monthly.
SNMMI | Society of Nuclear Medicine and Molecular Imaging
1850 Samuel Morse Drive, Reston, VA 20190.
(Print ISSN: 0161-5505, Online ISSN: 2159-662X)

SNMMI SOCIETY OF NUCLEAR MEDICINE AND MOLECULAR IMAGING